

Chirality effect on the global structure of spiral-domain patterns in the two-dimensional complex Ginzburg-Landau equation

Meng Zhan,^{1,*} Jinming Luo,^{1,2} and Jihua Gao³

¹Wuhan Institute of Physics and Mathematics, Chinese Academy of Sciences, Wuhan 430071, China

²Graduate School of the Chinese Academy of Sciences, Beijing 100049, China

³School of Materials, Shenzhen University, Shenzhen 518060, China

(Received 12 October 2006; published 24 January 2007)

It is well known that in the single-spiral-stable parameter regimes of the two-dimensional complex Ginzburg-Landau equation, spiral-domain patterns spontaneously appear. These patterns are disordered cells of frozen spiral waves well separated by thin walls (shocks), and to a good approximation, the walls are segments of hyperbolas. In this paper, we take a closer look at the global structure of spiral-domain patterns by using rigorous mathematical analysis and considering the unusual effect of the chirality (handedness) of spiral wave. An equation that determines the slope of the shock line is derived. We generalize this analytical method to study the interaction of a pair of spirals with different rotation frequencies, and obtain the geometrical structures of the shock line and the wave front of the invasion wave in transient processing.

DOI: 10.1103/PhysRevE.75.016214

PACS number(s): 05.45.-a, 82.40.Ck, 47.54.-r

I. INTRODUCTION

The complex Ginzburg-Landau equation (CGLE) is often recognized as a useful means to study the slow modulations of oscillations in the vicinity of a Hopf bifurcation [1,2]. The CGLE models both the qualitative and some quantitative features of a diverse variety of phenomena, such as the Belousov-Zhabotinsky (BZ) chemical reaction, the Rayleigh-Benard convection, and the Bose-Einstein condensation, etc. Therefore, it is only natural that there is extensive literature on the different parameter regimes of the CGLE, to characterize the spatiotemporal patterns, which can be classified as (1) defect-mediated turbulence, which is characterized by the topological defects of disordered spirals, which are continuously created and annihilated [3], (2) phase turbulence, which is devoid of any defect [1], and (3) the spiral-domain pattern, which is characterized by disordered cells of effectively frozen spirals separated by thin walls (shocks), and is also termed the frozen state, cellular pattern, and vortex glass state, etc. [4–7]. The simulations in Ref. [1] have provided some evidence that phase turbulence breaks down in the infinite-size, infinite-time limit. In all the above three types of spatiotemporal behaviors, point defects of the spirals play a dominant role in determining the system's dynamical behavior.

In Ref. [6], Bohr, Huber, and Ott (BHO) have intensively studied the local and global structures of shock lines, and found that locally each domain boundary (the shock line) is a segment of hyperbola with two nearest spiral tips as foci. This was achieved by using the phase approximation and considering the phase-matching condition. In this regard, the global structure fundamentally differs from Voronoi constructions or soap films. The theory of BHO has been well tested (see Fig. 3 in Ref. [6]). However, as we know, one of the essential and important features of spiral waves is the

chirality (handedness), which can be easily identified by its winding direction, clockwise or counterclockwise. Thus one might intuitively think that the chirality could also influence the interaction of spirals and, further, determine their global structures. As an example, see the two patterns with opposite chiralities (the top panel) and same chiralities (the bottom panel) in Fig. 1, where the different structures (the slopes) of the shock lines are easily distinguishable. Throughout this paper, we will use a plus (circle) to denote the positive (negative) chirality at the tip.

In chemical experiments, pairs of spiral waves with opposite chiralities are usually generated by perturbation of an expanding target wave, to get a clean spiral. In this situation, Muller *et al.* [8] have observed two distinct phenomena in BZ reactions [8]: the symmetrical pair with mirror symmetry (similar to our simulation in the top panel of Fig. 1) and the asymmetrical one with one spiral lagging about $\pi/2$ behind the other. In the latter case, the shock line deviates from the middle vertical line and it is also incapable of being fitted with a hyperbola. It would be interesting to study these ob-

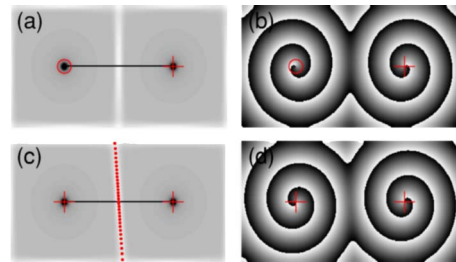


FIG. 1. (Color online) Snapshots of $|A|$ and $\text{Re}(A)$ on a 160×80 two-dimensional space with $\alpha=1.2$ and $\beta=0.0$, and zero-flux boundary conditions. The only difference between the upper and the lower panels is the chirality of the left spiral from different initial conditions, which results in a discernible change of the shock lines. Both patterns are stable. The dots in (c) obtained from the simulation of Eq. (5) fit the spatial position of the middle shock line very well.

*Electronic address: zhanmeng@wipm.ac.cn

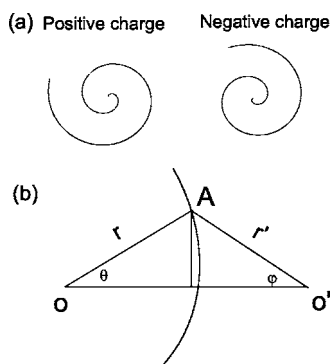


FIG. 2. (a) Schematic of positive and negative charges for the clockwise and counterclockwise chiralities. (b) Illustration for the formation of a shock line.

servations in theoretic means. To the knowledge of the authors, no explanation is available in the literature. Therefore, in this work we will study the global structure of the spiral-domain patterns (or specifically, the geometrical structure of the shock line from the collision of any two spiral waves), consider in detail the chirality effect, which might be a high-order effect, and explain the phenomena in simulations and experiments.

II. THE SIMULATION MODEL

Basic to the present investigations is the CGLE of the form

$$\frac{\partial A}{\partial t} = \mu_0 A - (1 + i\alpha)|A|^2 A + (1 + i\beta)\Delta A, \quad (1)$$

where the order parameter $A(x, y, t)$ indicates the complex field, and α and β are real constant parameters. The scaling number μ_0 is set to unity. An isolated spiral takes the form $A(r, \theta, t) = \rho(r) \exp\{i[-\omega t + \sigma\theta + \psi(r)]\}$, where (r, θ) are polar coordinates, ω is the rotation frequency of the spiral, and σ is the topological charge. $\sigma = (1/2\pi)\oint d\phi$, where ϕ denotes the phase surrounding the tip of the spiral. The topological charge $\sigma = +1$ (-1) results in a phase change $2\pi\sigma$ of A for a counterclockwise (clockwise) rotation around the tip center. We schematically show the positive and negative charge cases in Fig. 2(a). In the CGLE, spiral solutions with $\sigma \neq \pm 1$ are unstable. The real functions $\rho(r) = |A|$ and $\psi(r)$ have the following asymptotic behaviors: $\rho(r) \sim \psi' \sim r$ as $r \rightarrow 0$, and $\rho(r) \rightarrow \sqrt{1-k^2}$, $\psi' \rightarrow k$ as $r \rightarrow +\infty$, where k is the wave number of the spiral.

Figure 2(b) illustrates the interaction of a pair of spirals, whose tips are located at points O and O' and separated over a distance R , and the formation of the shock line with a curve in the middle region. Because the spiral in the far-field region can be well approximated with an Archimedean spiral (the Archimedean phase approximation), we have $\Phi_{AO} = \sigma_O \theta + kr + C_O - \omega t$ and $\Phi_{AO'} = \sigma_{O'}(\pi - \varphi) + kr' + C_{O'} - \omega t$, where σ_O and $\sigma_{O'}$, which can be $+1$ or -1 , are the charge numbers of the left and right spirals, respectively, and C_O and $C_{O'}$ are the phase constants. The wave number k is iden-

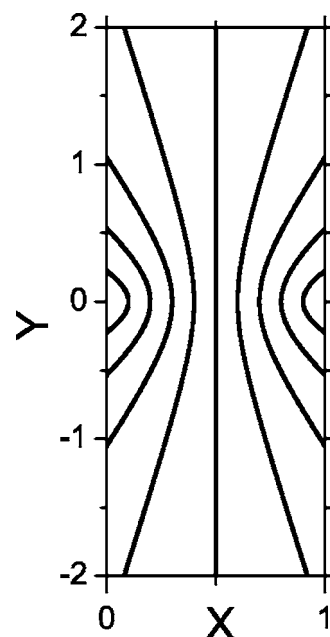


FIG. 3. The hyperbolic shock line structure from the BHO theory [or our analysis with $\sigma_O = \sigma_{O'} = 0$ in Eq. (5)].

tical for both spirals as here we consider a homogeneous system. On the shock lines, the phase of two spirals are equal modulo 2π , i.e., $\Phi_{AO} = \Phi_{AO'} \pmod{2\pi}$ (the phase-match condition). Consequently, we have $\Delta\Phi = \Phi_{AO} - \Phi_{AO'} = \sigma_O \theta + \sigma_{O'} \varphi + k(r - r') + C_O - C_{O'} - \sigma_{O'} \pi = 2\pi l$, with l being an integer; This relationship is satisfied for all points on the shock line. Bohr *et al.* [6] assumed that the distance from each spiral to the shock is much larger than the characteristic wavelength $\lambda = 2\pi/k$, and got $r - r' = \text{const}$, where the constant can be measured by the distances to any one point on the shock line for each pair of spirals. As a result, the shocks are viewed as segments of hyperbolas with the two nearest vortices as foci in their theory.

From the above analysis, apparently the influences of the chiralities of a pair of spirals (σ_O and $\sigma_{O'}$) have been ignored. To include the impact of chirality, we conduct a rigorous mathematical analysis by the implicit function theorem. With geometrical relations, we find

$$\varphi(r, \theta) = \arctan\left(\frac{r \sin \theta}{R - r \cos \theta}\right),$$

$$r'(r, \theta) = \sqrt{(r \sin \theta)^2 + (R - r \cos \theta)^2}. \quad (2)$$

Both φ and r' can be expressed as a function of (r, θ) , so the same as $\Delta\Phi$. $\Delta\Phi = \Delta\Phi(r, \theta)$. Thus, we have

$$\frac{\partial \Delta\Phi}{\partial r} dr + \frac{\partial \Delta\Phi}{\partial \theta} d\theta = 0. \quad (3)$$

The values of $\partial\varphi/\partial r$, $\partial\varphi/\partial\theta$, $\partial r'/\partial r$, and $\partial r'/\partial\theta$ can be easily calculated as follows:

$$\frac{\partial \varphi}{\partial r} = \frac{R \sin \theta}{(r \sin \theta)^2 + (R - r \cos \theta)^2},$$

$$\frac{\partial \varphi}{\partial \theta} = \frac{r(R \cos \theta - r)}{(r \sin \theta)^2 + (R - r \cos \theta)^2}, \quad \frac{\partial r'}{\partial \theta} = \frac{Rr \sin \theta}{\sqrt{(r \sin \theta)^2 + (R - r \cos \theta)^2}}. \quad (4)$$

$$\frac{\partial r'}{\partial r} = \frac{r - R \cos \theta}{\sqrt{(r \sin \theta)^2 + (R - r \cos \theta)^2}},$$

By putting the above equations into Eq. (3) and applying a scaling transformation, we obtain

$$\frac{dr}{d\theta} = \frac{-\sigma_O - \sigma_{O'} \frac{r(\cos \theta - r)}{(r \sin \theta)^2 + (1 - r \cos \theta)^2} + 2\pi m \frac{r \sin \theta}{\sqrt{(r \sin \theta)^2 + (1 - r \cos \theta)^2}}}{\sigma_{O'} \frac{\sin \theta}{(r \sin \theta)^2 + (1 - r \cos \theta)^2} + 2\pi m \left(1 - \frac{r - \cos \theta}{\sqrt{(r \sin \theta)^2 + (1 - r \cos \theta)^2}} \right)}, \quad (5)$$

where $m=R/\lambda$ ($\lambda=2\pi/k$) is the normalized distance of the two spirals scaled by the characteristic wavelength λ , and R is rescaled to be 1.

Hence, the chiralities of the two spirals (σ_O and $\sigma_{O'}$) come into Eq. (5) and determine the whole structure of the shock line. Given the charge numbers of the two spirals and the spatial positions of the two tips and any one point on the shock, we could reconstruct the whole curve from the integration of the above differential equation. If $\sigma_O = \sigma_{O'} = 0$,

$$\frac{dr}{d\theta} = \frac{r \sin \theta}{\sqrt{(r \sin \theta)^2 + (1 - r \cos \theta)^2} - (r - \cos \theta)} \quad (6)$$

should go back to the BHO theory and recover the hyperbolic structure, which has been well illustrated in Fig. 3. Here we used the standard fourth-order Runge-Kutta numerical integration scheme. Considering the chirality effect, in the top panel of Fig. 4, we plot the shock lines for ($\sigma_O = +1, \sigma_{O'} = +1$), ($\sigma_O = +1, \sigma_{O'} = -1$), and ($\sigma_O = -1, \sigma_{O'} = -1$), respectively, for $m=3$. The same case with $m=10$ is represented in the lower panel. Clearly the shock lines deviate from the hyperbolas in Fig. 3. If m is smaller, the degree of deviation gets larger and the chirality effect becomes more remarkable. A notable exception is the middle vertical line for the opposite chiralities in Figs. 4(b) and 4(e). Therefore, we can elucidate the different shock lines in the patterns of a pair of spiral waves with the negative-positive and positive-positive charges in Fig. 1; the dots in Fig. 1(c) from the computation of Eq. (5) are in good agreement with the realistic spatial position of the middle shock line. Another significant finding is that the deviation becomes greater for the likely charged case than the unlikely charged one [comparing Fig. 4(a) or 4(c) with Fig. 4(b)]. All these facets can be pictorially observed from the figures or mathematically analyzed from Eq. (5). Now, we focus our attention on the symmetries for all shocks. In Fig. 3, the hyperbolas have the left-right mirror symmetry, the up-down mirror symmetry, and the rotation symmetry with a rotation angle π (note that only two symmetries are independent), whereas a symmetry breaking happens after the chirality effect is considered: the symmetry due to rotation remains for the likely charged

cases [Figs. 4(a) and 4(c)], and the left-right mirror symmetry remains for the oppositely charged case [Fig. 4(b)]. We can fold Fig. 4(a) with $x=1/2$ (or $y=0$) to recover Fig. 4(c), and vice versa.

In Fig. 5, we compare our theory (the right panel) with the BHO theory (the left panel) in a real frozen state pattern. Periodic boundary conditions have been utilized. Without losing generality, we always choose the intersection point of

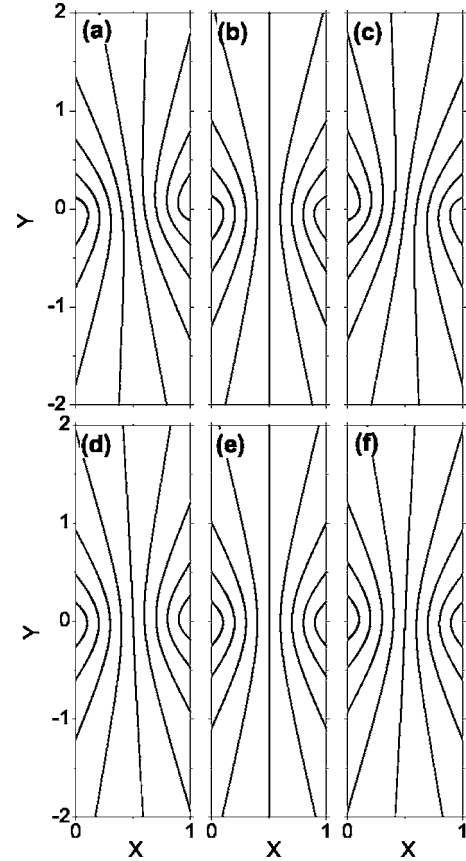


FIG. 4. The shock lines after considering the chirality effect in Eq. (5) for (a) $\sigma_O=1, \sigma_{O'}=1$, (b) $\sigma_O=1, \sigma_{O'}=-1$, and (c) $\sigma_O=-1, \sigma_{O'}=-1$, for $m=3$. (d), (e), and (f) are the same as the top panels, but with $m=10$.

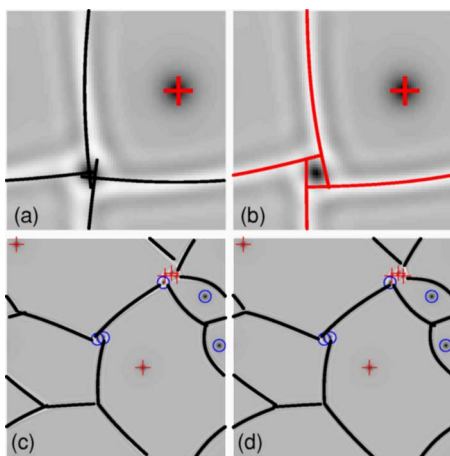


FIG. 5. (Color online) (a) and (c) The analytic positions for shock lines in the frozen state obtained from the previous BHO theory. (b) and (d) are the same as (a) and (c) including the effect of chirality. Two squared sizes with 40×40 (the upper panel) and 256×256 (the lower panel) points are considered. $\alpha=0.792$ and $\beta=-1$ as in Ref. [6].

the straight line connecting two nearest spiral tips and the shock curve as the initial integration point of Eq. (5). Figure 5(a) (or Fig. 3 in Ref. [5]) is a classical pattern constituted by a stable spiral and an edge vortex (sink) in the corner. Clearly our result in Fig. 5(b) with $\sigma_O=+1$ and $\sigma_{O'}=+1$ is much better than that in Fig. 5(a). Such a statement is valid for much larger sizes of spiral-domain pattern with several spirals [comparing the detailed structures in Figs. 5(c) and 5(d)], although now the relative distance (m) between two nearest tips are larger and the chirality effect is not as apparent as in the former case.

So far the only impact of the chirality on the global structure of spiral-domain patterns has become clear. Now, we extend the above analysis to analyze the geometrical structure of the shock line in transient processing of the interaction of two spiral waves with different frequencies [9–11]. In the study of the interaction of multiple (or simply two) spiral waves, it has been well accepted and understood that, initially, the spiral with the faster period of rotation can produce an approximately planar wave with an identical frequency, which intrudes (unwinds) into the domain of the slow one; after the unwinding, a drifting of the slower one to move out of the observed domain happens. In the first stage, the direct competition between the two spirals (similar to the case of spiral-domain patterns studied before) occurs in the transient time with a shock line gradually moving away from the faster spiral and into the slower spiral domain. Similar to Ref. [11], we study two spirals in a bipartite system separated by a middle division line, illustrated in Fig. 6(a), where we use a heavy curve to indicate the shock line and a thin line to denote the wave front of the invading planar wave. We have $\Phi_{BO}=\sigma_O\theta+k_1r+C_O-\omega_1t$ and $\Phi_{BO'}=\sigma_{O'}(\pi-\varphi)+k_2r'+C_{O'}-\omega_2t+k_i(R/2-r\cos\theta)$, after considering the phase relation between the points B and D. Note that the propagation direction of the invading wave is from right to left. Now k_1 , k_2 , and k_i are the wave numbers of the left spiral, the right spiral, and the invasion planar wave, respec-

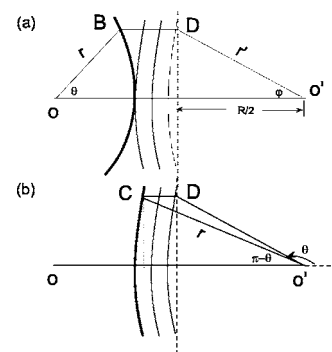


FIG. 6. Schematic illustrations for the shock line and the wave front of the invading wave in transient time.

tively, and they are all distinct. With $\varphi(r, \theta) = \arctan(2r \sin \theta/R)$ and $r'(r, \theta) = \sqrt{(R/2)^2 + (r \sin \theta)^2}$, by calculating $\partial\varphi/\partial r$, $\partial\varphi/\partial\theta$, $\partial r'/\partial r$, and $\partial r'/\partial\theta$, we have

$$\begin{aligned} \frac{\partial\varphi}{\partial r} &= \frac{2R \sin \theta}{R^2 + (2r \sin \theta)^2}, \\ \frac{\partial\varphi}{\partial\theta} &= \frac{2Rr \cos \theta}{R^2 + (2r \sin \theta)^2}, \\ \frac{\partial r'}{\partial r} &= \frac{2r \sin^2 \theta}{\sqrt{R^2 + (2r \sin \theta)^2}}, \\ \frac{\partial r'}{\partial\theta} &= \frac{2r^2 \sin \theta \cos \theta}{\sqrt{R^2 + (2r \sin \theta)^2}}. \end{aligned} \tag{7}$$

Under the assumption that the invading velocity is very slow, the shock line can be viewed as stationary, and finally by the implicit function theorem again we obtain

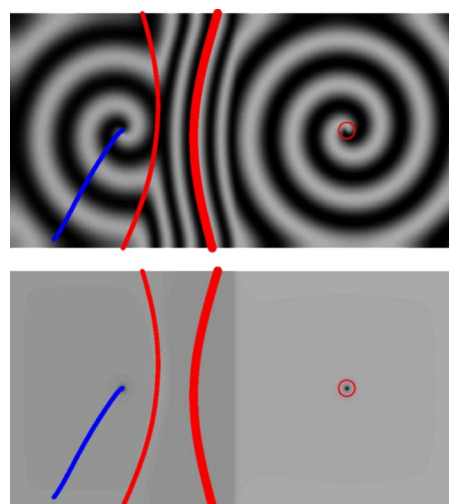


FIG. 7. (Color online) The patterns $\text{Re}(A)$ and $|A|$ for the interaction of a pair of spiral waves, where the right faster spiral is invading into the domain of the left slower one. Both the shock line and the wave front from the simulations of Eqs. (8) and (9) are in good agreement with the realistic situation.

$$\frac{dr}{d\theta} = \frac{-\sigma_{O'} - \sigma_{O'} \frac{2Rr \cos \theta}{R^2 + (2r \sin \theta)^2} + k_2 \frac{2r^2 \sin \theta \cos \theta}{\sqrt{R^2 + (2r \sin \theta)^2}} + k_i r \sin \theta}{\sigma_{O'} \frac{2R \sin \theta}{R^2 + (2r \sin \theta)^2} + k_1 - k_2 \frac{2r \sin^2 \theta}{\sqrt{R^2 + (2r \sin \theta)^2}} + k_i \cos \theta}. \quad (8)$$

Also we can apply the phase approximation to the analysis of the wave front of the invading wave [Fig. 6(b)]. $\Phi_{CO'} = \Phi_{DO'} + \Phi_{CD} = \sigma_{O'}[\pi - \arctan(2r \sin \theta/R)] + k_2 \sqrt{(R/2)^2 + (r \sin \theta)^2} + k_i(-r \cos \theta - R/2) + C_{O'} - \omega_2 t = 2\pi l$, with l being an integer. Accordingly,

$$\frac{dr}{d\theta} = \frac{-\sigma_{O'} \frac{2Rr \cos \theta}{R^2 + (2r \sin \theta)^2} + k_2 \frac{2r^2 \sin \theta \cos \theta}{\sqrt{R^2 + (2r \sin \theta)^2}} + k_i r \sin \theta}{\sigma_{O'} \frac{2R \sin \theta}{R^2 + (2r \sin \theta)^2} - k_2 \frac{2r \sin^2 \theta}{\sqrt{R^2 + (2r \sin \theta)^2}} + k_i \cos \theta}. \quad (9)$$

The numerical integration of Eqs. (8) and (9) in Fig. 7 would rebuild the curves of the shock line and the wave front of the invading wave at one time instance, given the positions of the two tips and any one point on the curve, and all constants $k_1=0.2210$, $k_2=0.2387$, $k_i=0.4916$, $R=128$, $\sigma_O=-1$, and $\sigma_{O'}=-1$. The two scaling parameters for the inhomogeneous bipartite system are $\mu_1=3.0$ and $\mu_2=3.5$; $\alpha=-0.4$ and $\beta=-1.5$; $\omega_0=0.4188$ and $k_0=2\pi/\lambda_0=2\pi/49.25=0.1276$ for $\mu_0=1.0$. For more details, see [11].

III. CONCLUSIONS AND BRIEF DISCUSSION

In conclusion, we have investigated the chirality effect of spiral on the global geometrical structure of shock lines of the frozen state in the homogeneous systems and the transient “frozen” state in the bipartite inhomogeneous systems. Explicit differential equations have been derived, which predict the shock lines very well. The method presented in this paper is expected to be applicable to other more complicated cases. Finally, we give some discussion. In a recent study, Brito *et al.* [7] found that the spirals in the so-called frozen state actually evolve extremely slowly, i.e., the frozen state is not truly frozen. In our observations, the drifting phenomenon is not observable in our still short evolution time with several hundreds of spiral rotations. Therefore, the frozen state can be viewed as static in most conditions, and our theory is still workable. Second, in a series of papers by Aranson *et al.* [12], they have established a theory of inter-

action for bound states of spiral waves in oscillatory media, which describes the direct, strong interaction of the tips of two spirals, whose distance is usually within one or two wavelengths. However, it fundamentally differs from ours, which mainly explores the case for sufficiently long distance, as the phase approximation is not applicable to the spiral core regime. Correspondingly, the curling shocks very close to the tips in Fig. 4 might be unreliable. Third, very recently the direction of propagation of spiral waves has received much attention, and a novel inwardly rotating spiral, termed an antispiral, has been found in both the BZ reaction and the CGLE model [13,14], in contrast to the usual outwardly rotating spiral. Here we should emphasize that the chirality (the handedness in spatial structure) is basically different from the normal spiral (or antispiral) property, which indicates the direction of propagation with time. We can recognize the chirality from a snapshot of the spiral pattern, but distinguish the spiral from the antispiral only from a sequence of patterns. In the CGLE, the stable spiral (or antispiral) is determined by the parameters α and β , whereas the chirality is controlled by the initial conditions. Importantly, Eq. (5) tells us that the propagation direction does not change the structure of the shock line, but the chirality does. Fourth, our analysis heavily depends on the phase approximation of spiral waves, which has been found very useful. In fact, we have generalized the phase approximation of spiral waves in the CGLE to describe the complex-oscillatory spiral waves [15], proposed an Archimedean spiral splay field theory, and successfully reconstructed the shape of the line effect, which is believed to be one of the generic features in complex-oscillatory spirals.

ACKNOWLEDGMENTS

This work was partially supported by the foundation of Wuhan Institute of Physics and Mathematics under Grant No. T06S607, and the National Natural Science Foundation of China under Grant No. 10675161. The work of J.G. was supported by the National Natural Science Foundation of China (No. 10405018). The authors thank Dr. B. S. V. Patnaik for his comments and help.

[1] H. Chate and P. Manneville, *Physica A* **224**, 348 (1996).

[2] I. S. Aranson and L. Kramer, *Rev. Mod. Phys.* **74**, 99 (2002).

[3] P. Couillet, L. Gil, and J. Lega, *Phys. Rev. Lett.* **62**, 1619 (1989).

[4] G. Huber, P. Alstrom, and T. Bohr, *Phys. Rev. Lett.* **69**, 2380 (1992).

[5] I. S. Aranson, L. Aranson, L. Kramer, and A. Weber, *Phys. Rev. A* **46**, R2992 (1992).

- [6] T. Bohr, G. Huber, and E. Ott, *Physica D* **106**, 95 (1997).
- [7] C. Brito, I. S. Aranson, and H. Chate, *Phys. Rev. Lett.* **90**, 068301 (2003).
- [8] S. C. Muller and T. Plesser, in *Chemical Waves and Patterns*, edited by R. Kapral and K. Showalter (Kluwer, Dordrecht, 1995), Chap. 2, p. 69.
- [9] V. I. Krinsky and K. I. Agladze, *Physica D* **8**, 50 (1983).
- [10] M. Hendrey, E. Ott, and T. M. Antonsen, Jr., *Phys. Rev. Lett.* **82**, 859 (1999).
- [11] M. Zhan, X. G. Wang, X. F. Gong, and C.-H. Lai, *Phys. Rev. E* **71**, 036212 (2005).
- [12] I. S. Aranson, L. Kramer, and A. Weber, *Phys. Rev. E* **47**, 3231 (1993); *Phys. Rev. E* **48**, R9 (1993).
- [13] V. K. Vanag and I. R. Epstein, *Science* **294**, 835 (2001).
- [14] Y. Gong and D. J. Christini, *Phys. Rev. Lett.* **90**, 088302 (2003); L. Bruschi, E. M. Nicola, and M. Bar, *ibid.* **92**, 089801 (2004).
- [15] M. Zhan and R. Kapral, *Phys. Rev. E* **72**, 046221 (2005).